Journal of Magnetic Resonance **142,** 300–312 (2000)
doi:10.1006/jmre.1999.1952, available online at http://www.idealibrary.com on IDEAL®

Ultrawide Band Multifrequency High-Field EMR Technique: A Methodology for Increasing Spectroscopic Information

A. K. Hassan,*[,1] L. A. Pardi,*[,2] J. Krzystek,* A. Sienkiewicz,† P. Goy,‡ M. Rohrer,*[,3] and L.-C. Brunel*[,4]

*Center for Interdisciplinary Magnetic Resonance, National High Magnetic Field Laboratory, Florida State University, 1800 E. Paul Dirac Drive, Tallahassee, Florida 32310; †Institute of Physics, Polish Academy of Sciences, Al. Lotników 32/46, 02-668 Warsaw, Poland; and ‡Laboratoire Kastler-Brossel, Département de Physique de l'Ecole Normale Supérieure, 24 rue Lhomond, F-75231 Paris Cedex 05, France

Received June 16, 1999; revised October 8, 1999

We report methodology that combines an ultrawide band multifrequency microwave system with technology of high magnetic fields for solving challenging problems in electron magnetic resonance (EMR) spectroscopy. This strategy has been made possible due to a novel EMR facility operating in an exceptionally wide range of microwave frequencies of 24 GHz to 3 THz, at magnetic fields up to 17 T, and in the temperature range of 1.6 to 330 K. The basic configuration of the multifrequency system works in a transmission mode and employs oversized cylindrical waveguides for routing the microwave power. A wide-band, low-noise, liquid helium cooled (4.2 K) InSb bolometer is used for signal detection. This approach results in an extremely wide-band performance, thus making it possible to employ a variety of solid-state millimeter and submillimeter microwave sources in combination with a far infrared laser microwave source for performing multifrequency EMR experiments. A complexity of resonant structures and related technical problems such as microphonics at high magnetic fields is virtually eliminated. The system is simple, yet sensitive, and has been revealed to be extremely advantageous while solving such problems as observation of AFMR transitions in spin-ordered systems, *g*-factor resolution enhancement in complex organic radicals, and resonance signal detection in EMR-silent spin systems having integer spin and large zero field splitting. A technical description of the multifrequency high-field EMR facility is presented and results of its performance tests are given. The potential utility of using the multifrequency high-field methodology in EMR studies is illustrated with selected examples of its recent applications. © 2000 Academic Press

Key Words: **broadband high-field EMR spectroscopy.**

I. INTRODUCTION

Electron magnetic resonance spectroscopy (EMR), a technique for studying paramagnetic, ferromagnetic, and antiferromagnetic spin systems, is a widely used tool in many fields of contemporary science, ranging from physics and chemistry to biology and medicine.

Traditionally, the EMR technique employed technical solutions and microwave frequencies corresponding to lower bands of the microwave electromagnetic spectrum. Commercially available and homebuilt EMR systems usually operate at microwave frequencies ranging from 3 GHz (S band) to 35 GHz (Q band) (*1, 2*). In the eighties, however, an increasing number of groups ventured into higher frequencies and fields (*3–7*). The past decade confirmed this trend; for a fairly recent review see, for example, Ref. (*8*). The rationale for extending microwave radiation frequency beyond lower microwave bands is a consequence of improved spectral resolution (*3, 4*) and higher overall sensitivity at corresponding higher magnetic fields (*9, 10*). The high-field technology makes it also possible to reach non-Kramers spin systems, i.e., integer spin systems having large zero field splitting (*11–13*). Such spin systems are often EMR-silent at conventional low microwave frequencies and low magnetic fields. Recently, several authors have reviewed technical aspects and advantages of application of high-field EMR (HF-EMR) technique to numerous spin systems (*14–16*).

It is customarily accepted that EMR spectrometers performing at frequencies higher than 90 GHz are referred to as high-field EMR systems. The advent of the HF-EMR technique has been made possible due to improvements in the design of superconducting magnets for nuclear magnetic resonance spectroscopy. Superconducting magnets fulfilling the requirements of high stability and reasonably high homogeneity in conjunction with the ability for fast sweeps at magnetic fields up to 17 T are becoming commercially available. Due to a significant progress in the design of resistive magnets, the highest magnetic fields available for the cw high-field EMR spectroscopy have recently been extended to 25 T (*17*). With the use of resistive-pulsed (*18*) and hybrid (*19*) magnets even higher field intensities can be obtained and employed in HF-EMR spectroscopy. However, the latter magnets are by far more compli-

[1] Present address: Service National des Champs Intenses, C.N.R.S. 25 Avenue des Martyrs, F-38042 Grenoble Cedex, France.

[2] Present address: Istituto di Fisica Atomica e Molecolare—CNR, via del Giardino 7, I-56127 Pisa, Italy.

[3] Present address: Institut für Physikalische und Theoretische Chemie, Universität Frankfurt, Marie-Curie Strasse 11, D-60439 Frankfurt, Germany.

[4] To whom correspondence should be addressed. Fax: (850) 644-1366, E-mail: brunel@magnet.fsu.edu.

1090-7807/00 $35.00
Copyright © 2000 by Academic Press
All rights of reproduction in any form reserved.

cated in use and have poorer resolution properties than the superconducting solenoids.

Historically, the first HF-EMR spectrometers operated at the microwave frequencies from the lower register (70–170 GHz) of the millimeter microwave range. High-frequency klystrons (*4, 20*), backward wave oscillators (*21*), and harmonic generator crystals (*22*) were used for generating millimeter microwave radiation in these early HF-EMR systems. Over the past 15 years a considerable number of homemade high-field cw and pulsed EMR spectrometers have been designed. Generally, these systems operate around certain chosen frequencies, such as 94 GHz (*4, 23*), 140 GHz (*20*), 250 GHz (*6, 24*), or 360 GHz (*25*). In particular, the commercial availability of certain crucial elements, such as waveguides, and the well-developed technology of 94-GHz solid-state microwave sources made W-band EMR systems especially popular. Recently, Bruker Analytik GmbH commercialized a 94-GHz system (*26, 27*).

Although the potential of possible applications of the multifrequency (MF) approach in combination with high-field EMR spectroscopy had been early and widely recognized, MF HF-EMR systems have not become very popular. Their development has long been restricted by the lack of reliable and easy way to operate microwave sources in millimeter and submillimeter frequency ranges. Furthermore, employment of traditional waveguide-based techniques for microwave propagation has become increasingly difficult at frequencies higher than 100 GHz. At such high frequencies, single-mode rectangular waveguides are becoming excessively lossy, with their theoretical propagation loss being of $\sim$3 and $\sim$12 dBm^{-1} at 100 and 250 GHz, respectively (*28*). The experimentally observed insertion loss of monomodal waveguides can be even higher due to imperfections and rapidly increasing surface resistivity of metallic walls with increasing frequency. This fact is of particular importance while designing the high-field EMR systems whose dimensions and corresponding microwave pathways are usually much longer than for traditional, low-field operating spectrometers.

Technical difficulties associated with the design of microwave propagation circuits operating within a large frequency range can be overcome by using overmoded transmission lines. Such oversized cylindrical waveguides reveal a tolerable insertion loss that is less than 1 dBm^{-1} for frequencies lower than 440 GHz (*29*). There is a large body of the literature data regarding successful applications of cylindrical oversized waveguides and avoiding resonant structures for microwave transmission and signal processing while performing multifrequency EMR measurements at high magnetic fields (*7, 13, 17, 19, 30–34*).

We explored the technology of overmoded waveguides while designing the multifrequency (24 GHz to 3 THz), high-field EMR spectrometer described in this paper. The lowest frequency range (from 24 to 130 GHz) was covered with a tunable YIG transistor oscillator. A set of solid-state microwave sources (Gunn oscillators) was used to cover the middle frequency range of the system (95 to 550 GHz). The upper frequency bands (up to 3 THz) are covered by a set of spectral lines of an optically pumped far infrared laser (FIR). The fundamental broadband configuration of the MF HF facility was based on the direct transmission of microwave radiation through the sample space. This greatly simplified the overall design of the microwave power pathway, since the technical complexity of either monomodal cavities or tunable Fabry-Pérot (FP) resonators was avoided. The microwave energy was simply routed from the microwave source to the sample location in the superconducting solenoid and finally to the detector using sections of oversized cylindrical waveguides and appropriately arranged metallic mirrors.

In spite of its simplicity, our MF HF-EMR system revealed itself to be extremely useful when applied to samples of nonlimited availability. In particular, it enabled one, for the first time, to observe a complete set of antiferromagnetic resonance (AFMR) modes in the magnetically ordered state of $KMnPO_4 \cdot H_2O$ and related layered manganese organic phosphonates (*33*). The capability of observing AFMR resonances in an exceptionally wide range of electromagnetic radiation frequencies, as well as using broad magnetic field sweeps, made it possible to accurately determine important parameters characterizing the magnetically ordered phase of this spin system. It should be stressed that these antiferromagnetically ordered systems, successfully studied with our multifrequency high-field apparatus, are EMR-silent at conventional frequencies and fields. Two other examples of the multifrequency high-field approach, including enhancement of the g-factor resolution for a complex organic radical, as well as EMR signal detection from a system having an integer spin ($S = 2$) and large zero field splitting, are also presented (Section IV).

It is worth noting that technical problems associated with the multifrequency operation of HF-EMR systems can also be overcome using a strategy that is based on a variety of quasi-optical (Q-O) techniques. The emerging technology and broader commercial availability of extremely low-loss and nondispersive quasi-optical elements such as broadband reflecting optics and corrugated waveguides seem to be particularly attractive for MF HF-EMR applications. The experimentally measured propagation loss of a straight section of the cylindrical corrugated waveguide was found to be only of 0.01 dBm^{-1}, compared to 4–5 dBm^{-1} for a high-quality single-mode waveguide at 90 GHz (*35*). Moreover, precise mode and phase control, similar to that known from low-frequency waveguide-based EMR devices, can be achieved in Q-O systems. Using the Q-O approach it is possible to design a high-frequency microwave bridge that can operate in an almost analogous way to well-known low-frequency microwave bridges, thus allowing for both amplitude and phase control in the spectrometer reference arm. A number of HF-EMR spectrometers employing the Q-O approach have already been built (*6, 24, 25, 35–37*). However, a truly multifrequency broadband

operation of such HF-EMR systems, comparable to that presented in this paper, has yet to be experimentally demonstrated.

Another recent approach for developing MF HF-EMR probes is based on the implementation of wide bandwidth dielectric resonators known as whispering gallery mode resonators (*38*). This promising technology offers a high merit factor, Q_L, that only slightly declines with increasing frequency. High filling factors can also be expected for such resonant sample probes, which will result in potentially high sensitivities over a wide frequency range. Nevertheless, practical applications of these novel devices are still necessary to prove their usefulness for multifrequency high-field EMR spectroscopy.

II. TECHNICAL OVERVIEW

A. Concept of the MF HF-EMR Spectrometer

The general outline of the MF HF-EMR system is shown in Fig. 1. The facility employs a 17-T superconducting magnet and a set of solid-state microwave sources covering the spectral range of 24 to 550 GHz. Incorporation of an optically pumped far infrared laser microwave source enables one to extend the upper frequency limit to 3 THz. The basic configuration of the spectrometer uses oversized cylindrical waveguides for transmission of the microwave power from the source to the sample space and for routing the transmitted power to the detector. It operates in the Faraday geometry with the microwave propagation parallel to the static magnetic field (B_0). This approach, already known in the literature as the "single-pass" configuration (*7*), implies fewer technological constraints, which are typical to single-mode propagation in rectangular waveguides. It suffers, however, from the low microwave power level at the sample position compared to the systems containing resonant structures. Generally, it is also more difficult to preserve and control polarization and phase of the propagating beam in the oversized cylindrical waveguide-based systems. However, for many cw EMR experiments these disadvantages are counterbalanced by the fact that the concentration sensitivity offered by the transmission-type systems remains high (*9*). Simplicity of the overall spectrometer design and virtual lack of microphonics are also strong arguments in favor of the transmission approach. The latter factor is of extreme importance while investigating spin systems having very broad linewidths that require large modulation for satisfactory sensitivity. The schematic outline of the single-pass transmission probe is shown in the central part of Fig. 1.

For small-size and spin-concentrated samples, as well as for lossy aqueous samples, we found it useful to implement a modified version of the transmission probe, i.e., a "double-pass" transmission probe (Section B of this chapter). In order to increase the absolute sensitivity of our MF HF-EMR facility for such samples we also designed a Fabry-Pérot resonator (*29*).

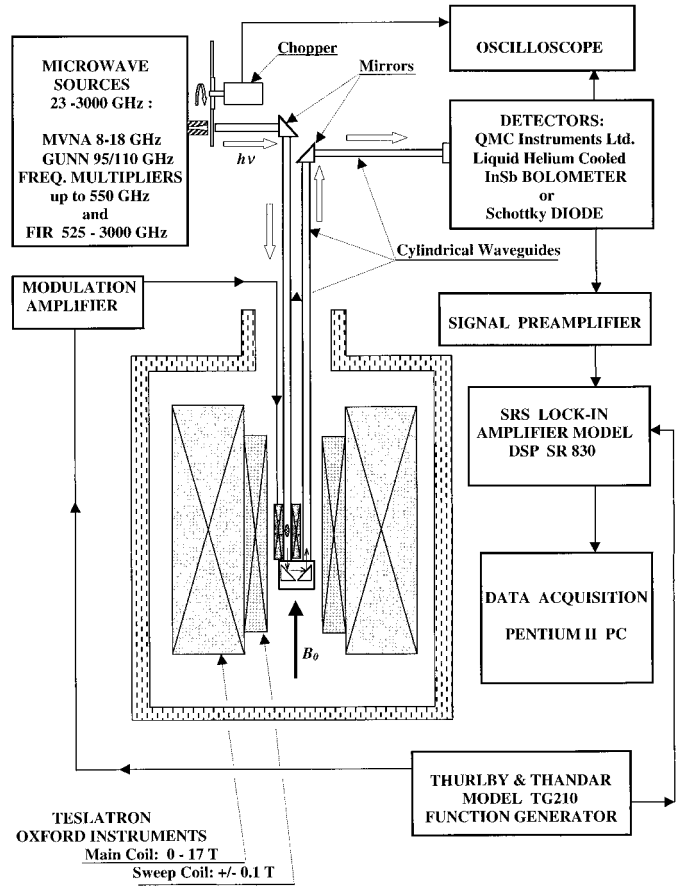

FIG. 1. Schematic diagram of the MF HF-EMR spectrometer operating in the single-pass transmission mode. Microwave power is transmitted through the sample compartment located in the central part of the superconducting solenoid. The continuous flow cryostat (VTI) that accommodates the transmission single-pass and double-pass probes or the FP resonator is not shown in this simplified diagram.

The other major features of the MF HF-EMR spectrometer depicted in Fig. 1 are microwave detectors, consisting of either a liquid helium cooled, broadband magnetically enhanced performance bolometer, Model QFI/3BI from QMC Instruments Ltd. (London, Great Britain), or Schottky diodes. In addition to recording conventional spectra (first harmonic of the magnetic field modulation frequency, absorption in-phase), the system makes it also possible to simultaneously monitor amplitude and phase of EMR signals. This latter feature is achieved without magnetic field modulation when using a Millimeter Vector Network Analyzer (MVNA), Model No. MVNA-8-350 from AB Millimètre (75005 Paris, France) for the front-end signal processing. A detailed description of the vector detection system applied for recording EMR spectra can be found in Ref. (*39*). For acquiring conventional cw EMR spectra the field modulation (~10 kHz) is provided by a function generator, Model No. TG210, manufactured by Thurlby & Thandar. Before energizing the modulation coil, the modulation signal is fed into a MOS-FET current amplifier, Model No. X-820HD

(Analogue Associates). The cylinder-shaped, 50-mm-long modulation coil was wound around a fiberglass-made (G-10) mandrel. In order to eliminate microphonics, the modulation coil was tightly fitted to the lower section of the stainless steel cylindrical waveguide. This part of the waveguide is located in the most homogeneous section of the magnetic field and accommodates the sample compartment and sample holder. The modulation coil delivers the modulation field amplitude up to 2.5 mT at 10 kHz.

Generally, the QMC bolometer is used for detection when conventional cw EMR field-swept spectra are recorded. After detection and preamplification, the signal is fed into a phase-sensitive detector. A lock-in amplifier (Model No. DSP SR830 from Stanford Research Systems, Inc., Sunnyvale, CA) is used to single out and process the signal component that corresponds to the field modulation frequency. EMR spectra are monitored and stored in a Pentium 233-MHz PC computer. The PC-based data acquisition system runs using a homewritten software that works within the LabVIEW (National Instruments) 4.1 environment. A standard GPIB board is used for retrieving data from the lock-in amplifier. The serial port of the PC is used for communication with the magnet power supply and for monitoring the sample temperature.

We found it useful to monitor the total power incident on the detector during the microwave beam adjustments or while changing the microwave sources. For this purpose we used a variable frequency optical chopper, Model No. 300 from Scitec Instruments Ltd. (Redruth, Cornwall, England). The blade of the chopper was inserted into a gap between a section of the cylindrical waveguide and the tapered horn transition attached to the output of the microwave source. The amplitude-modulated signal from the detector was then fed into an oscilloscope, thus providing an easy way for monitoring the microwave power available from a given source.

The extension of the working frequency range while switching from the Gunn diode-based oscillators and appropriate harmonic generators to the FIR laser microwave source could be performed without any major modification of the spectrometer configuration. Independent of the microwave source used for a given experiment or the probe type, the microwave power could be routed to the sample space using the same cylindrical oversized waveguide circuitry.

As mentioned before, the spectrometer incorporates a set of different microwave sources that can be combined with different signal detectors (see also Fig. 1). Depending on application, the EMR system can be assembled using one of the following configurations:

(1) a Gunn diode oscillator as a microwave source in combination with bolometeric detection and modulation of the magnetic field;

(2) the MVNA synthesizer and harmonic generator as a microwave source with bolometeric detection and modulation of the magnetic field;

(3) the MVNA synthesizer and harmonic generator as a microwave source and a corresponding Schottky diode detector (no modulation of the magnetic field);

(4) a Gunn oscillator as microwave source and a corresponding Schottky diode combined with the MVNA for detection (no modulation of the magnetic field);

(5) the FIR laser with the bolometer as a detector and modulation of the magnetic field.

The last configuration (5) mostly used in combination with a different, high-resolution 25-T resistive magnet was described in Ref. (*17*). A brief characterization of the above-mentioned spectrometer configurations is presented in Section III. For acquiring conventional field-swept cw EMR spectra, the first configuration (1) of the MF HF-EMR facility is mostly used.

B. Spectrometer Components

1. Magnet system. Magnets that are able to deliver homogeneous and stable magnetic field of large intensity are prerequisite for the HF-EMR technology. The HF-EMR system operational at the NHMFL in Tallahassee, Florida, was built around a prototype commercial superconducting 17-T magnet, Teslatron from Oxford Instruments (Witney, Oxon, England). This magnet contains two sets of coils: (1) the main set of coils used for setting the fundamental component of the Zeeman field or for generating large field scans (up to 17 T) and (2) the sweeping coil producing the magnetic field sweep that is necessary for performing conventional high-resolution cw EMR experiments.

The main set of coils of the Teslatron magnet consists of a number of coaxial solenoid sections wound with Nb_3Sn and NbTi superconducting filamentary wires. It can reach the maximum field of 15 T at 4.2 K and of 17 T when cooled to 2.2 K using a lambda plate. The field homogeneity at 14.5 T is better than 1×10^{-5} within a cylinder of 1 cm in diameter and 1 cm in height. The maximum sweeping rate of the main coil is 0.5 T/min at 4.2 K and 0.15 T/min at 2.2 K. The current decay rate of the magnet while in persistent mode is of the order of 5 ppm/h. The sweep coil allows for ± 0.1 T sweeps around the field set by the main coil. The maximum sweep rate of the sweep coil is 0.12 T/min. The helium evaporation rate is 0.3 L/h when the magnet operates in the persistent mode at 4.2 K, becoming more pronounced when operating in nonpersistent mode. The liquid helium consumption at 2.2 K is 5 L/h. Power to the main coil and to the sweeping coil is delivered from two Oxford Instruments-made superconducting magnet power supplies, Model No. IPS180-20 and Model No. IPS120-10, respectively.

2. Microwave sources. Multifrequency operation across a wide range of millimeter and submillimeter frequencies of our HF-EMR system was made possible by using a set of different microwave sources. Continuous coverage of the lowest frequency range from 24 to ca. 130 GHz is provided by the

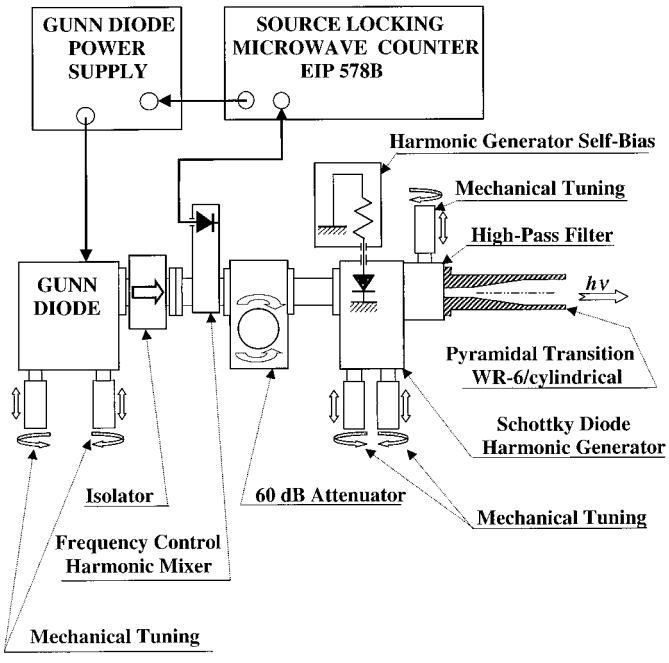

FIG. 2. Schematic diagram illustrating the design of the 110-GHz (ESA1-110) and 95-GHz (ESA1-95-5) Gunn diode-based microwave sources employed in the MF HF-EMR system. The pyramidal transition, the WR-6 rectangular/overmoded cylindrical waveguide, for the 110-GHz operating device is to be substituted by the pyramidal transition, and the WR-10/overmoded cylindrical waveguide for the 95-GHz operating source, respectively.

MVNA. Microwave frequencies in the range of 8–18 GHz are produced in the MVNA's internal quartz-stabilized yttrium iron garnet oscillator and subsequently fed into a Schottky diode harmonic generator which acts as a frequency multiplier. Although available from the MVNA, the frequency range of 8 to 24 GHz has no practical application since the cylindrical waveguide circuitry used in our system becomes excessively lossy at frequencies lower than 24 GHz. The intermediate frequency region (from 92 to 550 GHz) is covered using two Gunn oscillators manufactured by AB Millimètre, Model Nos. ESA1-95-5 and ESA1-110. These microwave sources have their nominal operating frequencies centered around 95 and 110 GHz and are mechanically tunable within their specific intervals of 92 to 98 GHz and of 107 to 113 GHz, respectively. Higher frequencies are obtained by frequency multiplication. Therefore, each of the Gunn diode oscillators is equipped with a Schottky diode harmonic generator. A block diagram of the 110 GHz operating source, ESA1-110, is shown in Fig. 2. The outline of the 95-GHz operating source is similar. Both sources are also equipped with a set of exchangeable high-pass filters adjusted for different frequency bands. For the 110-GHz source, these high-pass frequency bands are 220, 330, 440, and 550 GHz, whereas for the 95-GHz source, the high-pass frequency bands are 190, 285, 380, and 475 GHz. The high-pass output filters permit lower harmonics to be cut off, depending on the frequency of interest. The operating frequencies of the Gunn oscillators are measured, and frequency locked to a source locking microwave counter, Model No. EIP 578B from EIP Microwave, Inc. (Milpitas, CA). The resulting nominal stability of the fundamental frequency is determined by the stability of the EIP timer which is better than 1×10^{-10} rms, i.e., about 10 Hz for 1 s averaging time. In practical operation, we have observed a long-term source stability of the order of 1 kHz when locked to the counter.

The highest frequency register of our MF HF-EMR facility is provided by a CO_2 pumped far infrared laser, Model No. FIRL100, from Edinburgh Instruments Ltd. (Edinburgh, Great Britain). It offers a series of discrete frequencies starting from 158 GHz up to 7.5 THz. However, because of the low output power of the FIRL100 at lower frequencies and sharply decreasing sensitivity of the bolometer detector at the high-frequency end, the infrared laser-based microwave source is mainly used to span the high-frequency range of 525 GHz to 3 THz. Compared to the solid-state microwave sources used in our system, the FIR laser source has much higher amplitude and phase noise levels. The infrared laser source also suffers from the lack of tunability and substantial complexity of operation and maintenance.

The characteristic frequency bands and corresponding microwave power levels available from different sources of our MF HF-EMR spectrometer are listed in Table 1, according to Ref. (*40*).

3. Microwave detectors. Depending on the application and frequency of operation of our MF HF-EMR spectrometer, the front end of the signal detection processing consists of either a bolometer or a Schottky diode. The bolometric option employing the QFI/3BI liquid helium cooled fast InSb hot-electron bolometer provides signal detection with a particularly high sensitivity with the noise equivalent power (NEP) of 10^{-13} W/$\sqrt{\text{Hz}}$. At 4.2 K its response time is $\sim 1\ \mu$s, which makes it fast enough to allow for field modulation frequencies up to 1 MHz. While this type of detector offers both fast and sensitive

TABLE 1
Frequency Range and Output Power Available from the Different Microwave Sources

Source	Frequency [GHz]	Power [mW]
MVNA	8–130	10–0.01
Gunn 95 GHz	95	52
	190	3.6
	285	1.2
	380	0.6
	475	0.24
Gunn 110 GHz	110	42
	220	3.7
	330	1.7
	440	0.96
	550	0.18
FIR laser	158–7500	0.1–200

cw detection, its limitation is in its sharply decreasing sensitivity outside the frequency range of 70 GHz to 1.5 THz.

As mentioned before, Schottky diodes represent another alternative for detection. While they are faster than bolometers and do not need to be cryogenically cooled, their sensitivity is at least one order of magnitude lower, with a maximum NEP around 10^{-12} W/$\sqrt{\text{Hz}}$ (*40*). In the case of our MF HF-EMR system the Schottky diodes detectors were exclusively used in combination with the MVNA-assisted vector detection when we found it convenient to simultaneously acquire amplitude and phase-related changes of the EMR signal.

4. Propagation elements and sample probes. We used sections of brass-made tubes (10.0-mm ID and 12.0-mm OD) of appropriate length for manufacturing all parts of the microwave pathway outside of the cryostat. These mainly horizontal waveguide elements were employed to span the distance from the microwave source to the probe and from the probe to the detector entrance. In order to minimize the thermal loading while working at low temperatures, we used thin-wall (10.0-mm OD, 9.6-mm ID, and 0.2-mm wall thickness) stainless steel tubes to assemble the cryogenic inserts of both probes. Heat radiation shields made of circular copper plates were attached to the stainless steel waveguides to protect against room temperature radiation when working at lower temperatures. These elements, attached to the waveguides by means of miniature brass-made brackets, also provided mechanical stiffness to the cryogenic part of the sample insert.

The microwave pathway of the single-pass transmission probe contains four deflecting 45° mirrors made of optically polished brass. The location of these mirrors is shown in Fig. 1. Two such mirrors are located under the sample space, in the bottom part of the probe. The outline of this portion of the single-pass probe is shown in Fig. 3a. The mirrors are built into the lower bracket that was made of nonmagnetic brass. This bracket, in its upper part, is equipped with two cylindrical entrances and precise cylindrical clamps that snap on the waveguide terminations. Such a design makes it possible to easily detach the bracket from the lower part of the waveguides, thus allowing for a quick sample exchange. The latter procedure can be performed when the probe is removed from the magnet. Cylindrical-shaped sample compartments made of PTFE (9.5-mm OD, 9.0-mm ID, and 10.0-mm height) are used to hold samples. The sample compartments can accommodate either liquid or powdered samples up to 300 μL total volume. These sample-holding elements are snugly fit to the inner hole of the cylindrical waveguide and their vertical position can be precisely adjusted using short sections of thin-wall PTFE-made tubes.

The lowest part of the double-pass transmission probe is shown in Fig. 3b. This probe also operates in the Faraday geometry. In contrast to the single-pass transmission probe, the double-pass probe contains only one vertical waveguide section for routing microwave power to and from the sample. A

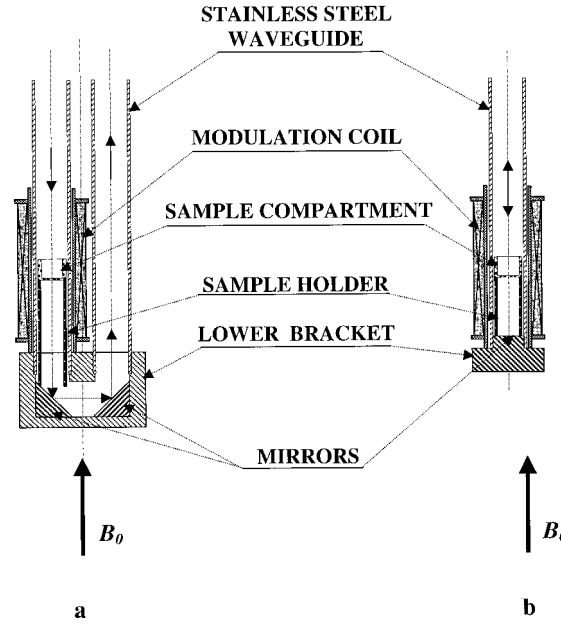

FIG. 3. Cross-sectional view of the lower section of the transmission probes. (a) Outline of the lower part of the single-pass transmission probe. (b) Outline of the lower section of the double-pass transmission probe.

flat mirror reflecting back the microwave power transmitted through the sample terminates the lower end of the stainless steel waveguide section. The sample is exposed to the microwave power twice, since the beam transmitted through it is reflected back to the sample by the bottom mirror. The process of the sample positioning in this probe is similar to that used for the single-pass system. If necessary, the sample compartment can also be positioned directly on the planar mirror. The total length of both probe heads, as measured from the cryostat upper flange to the sample location in the center of the superconducting solenoid, is 95 cm.

To increase the spectrometer sensitivity, a Fabry-Pérot resonator was designed for multifrequency operation in the frequency range of 110 to 330 GHz. The tunable semiconfocal arrangement included an inductive copper mesh (upper resonator mirror) and a spherical metallic mirror that was located at the bottom of the resonant structure. Both mirrors were mechanically adjustable to ensure the best performance in the entire temperature range from room temperature to 4.2 K. Frequency tuning of the FP resonator was achieved by high-precision axial adjustment of the lower reflection mirror. Detailed technical description of this newly developed resonator appeared elsewhere (*29*). The FP resonator can easily be incorporated into the same magnet/VTI setup that is used for the single-pass and double-pass transmission probes. Since the FP resonator operates in the reflection mode, a single tube is used for guiding the incident and reflected microwave power in the cryogenic section of the probe.

There is a need to separate the incoming and outcoming beams while employing the double-pass transmission probe or

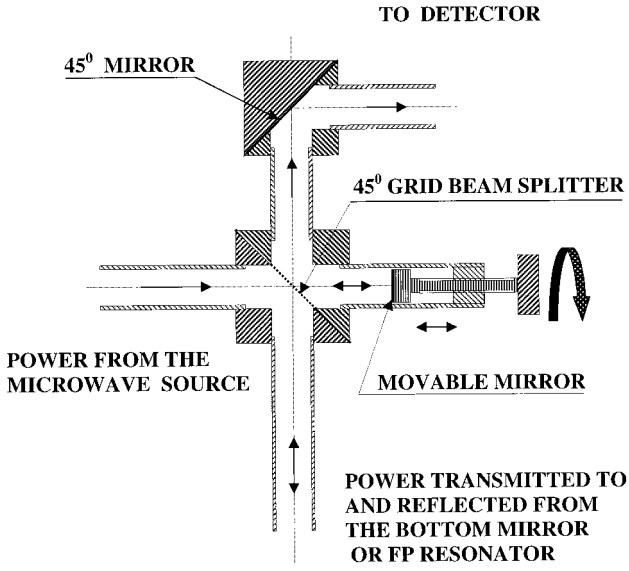

FIG. 4. Outline of the grid-based beam splitter that was used in combination with the double-pass transmission probe or with the FP resonator. A movable mirror in the reference arm provides fine phase control and is also used for changing the detector bias.

the FP resonator, since both devices operate in the reflection mode. In our experimental setup a beam splitter that is shown in Fig. 4 fulfills this function. One of the horizontal arms of the beam splitter is equipped with a movable mirror that is used for mixing a phase-adjusted biasing wave into the microwave power reflected from the sample. We found this feature to be very useful for precise phase adjustment and control of the detector polarization power. The phase adjustment that was provided by the movable mirror also made it easier to approximately get an absorption spectrum. Technical details of the design of the beam splitter can be found in Ref. (*29*).

The warm bore of our Teslatron is 61 mm in diameter and can easily accommodate a variable temperature insert (VTI), also made by Oxford Instruments, Model No. CF1200 DEG. The inner bore of the VTI is 38 mm in diameter, thus making it possible to accommodate either the transmission probes or the FP resonator. The VTI in combination with an Oxford Instruments-made Intelligent Temperature Controller Model No. ITC503 allows the temperature to be continuously varied around the sample space in the 1.6–330 K range with ± 0.1 K stability. The cooling is achieved by a continuous flow of cold gaseous helium taken from an external liquid helium container. The heater located at the bottom of the VTI provides a possibility of varying the sample temperature. The temperature inside of the VTI can also be monitored with a standard carbon glass resistor that is located above the heating element. An additional Cernox thermometer, placed outside the waveguide next to the sample position, was used to sense the temperature of the sample.

III. SPECTROMETER PERFORMANCE

1. Sensitivity

The sensitivity of the spectrometer varies depending on the configuration used. For configuration (1), i.e., employing the Gunn diode as the microwave source and the QMC bolometer for signal detection, sensitivity measurements were performed using the single-pass transmission probe. The following three different samples were used for these sensitivity tests:

(i) BDPA (α,γ-bisdiphenylene-β-phenylallyl benzene complex, Aldrich) in polystyrene film. For this sample, containing 9×10^{17} unpaired spins, we obtained the S/N ratio of 6×10^4 (the observed EMR linewidth was 1.64 mT). The spectrum was taken at 328.5 GHz at 273 K, with the instrumental time constant of 1 s. Spectra taken at 109.5 and 219 GHz showed similar S/N ratios.

(ii) DPPH (2,2-diphenyl-1-picrylhydrazyl, Sigma), ground to fine powder. The sample contained 3.2×10^{18} unpaired spins. The observed S/N ratio was of 8.6×10^4 (the linewidth was 0.6 mT). The spectrum was taken at 328.59 GHz at 273 K, with the instrumental time constant of 1 s. Spectra taken at 109.5 and 219 GHz revealed similar S/N ratios.

(iii) Phosphorus-doped silicon (Si:P). This sample contained 8×10^{12} unpaired spins. Its EMR spectrum is shown in Fig. 5. Two EMR features, 4.2 mT apart, correspond to the hyperfine splitting due to the phosphorus nuclear spin ($I = \frac{1}{2}$). The measured S/N ratio for this spectrum is 30. The linewidth of a single feature is 0.275 mT. This spectrum was acquired at 10 K using the third harmonic of the 110-GHz source (328.41 GHz), with 0.15 $\mathrm{mT}_{\text{p-t-p}}$ amplitude of 8-kHz field modulation. The instrumental time constant was 0.3 s.

The room temperature measurements for both BDPA and DPPH were repeated several times. The averaged results yielded a spectrometer sensitivity of $(4 \pm 3) \times 10^{12}$ spins/G · s. The 10 K tests performed for Si:P yielded the sensitivity of $(1.2 \pm 0.3) \times 10^{10}$ spins/G · s. The sensitivity results for the single-pass transmission configuration are summarized in Table 2.

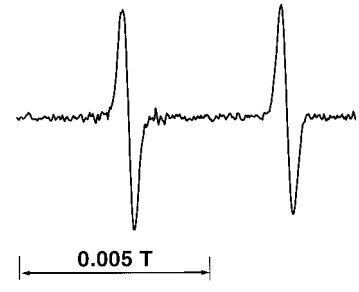

FIG. 5. EMR spectrum of phosphorus-doped silicon acquired at 10 K. Instrumental experimental conditions were microwave frequency, 328.41 GHz; field sweep rate, 1.8 mT/min; field modulation frequency, 8 kHz; modulation amplitude 0.15 mT; time constant, 0.3 s.

TABLE 2
Comparison of the Detectable Minimum Number of Spins for Different Polycrystalline Samples Measured Using the Single-Pass Transmission Configuration (Spectrometer Configuration 1)

Sample	Frequency [GHz]	Temperature [K]	Sensitivity [spins/G · s]
BDPA	330, 220, 110	273	$(4 \pm 3) \times 10^{12}$
DPPH	330, 220, 110	273	$(4 \pm 3) \times 10^{12}$
Si:P	330	10	$(1.2 \pm 0.3) \times 10^{10}$

Substantial sensitivity improvement of about two orders of magnitude, compared to the single-mode transmission mode experiments, was obtained using the FP resonator at 330 GHz (*29*). Sensitivities of the remaining transmission-type configurations (2, 3, and 4) of our HF-EMR system were also measured. We used the same polycrystalline DPPH sample as for sensitivity testing of the single-pass transmission setup (spectrometer configuration 1). The results of these comparative experiments are listed in Table 3.

As can be seen from the tabulated results, for the lowest frequencies of operation of our system (24 and 33 GHz), the spectrometer sensitivities are substantially worse compared to those obtained at higher frequencies (95 to 450 GHz). At such low frequencies, the MVNA has to be used as the microwave power generator. At the same time, Schottky diodes are employed for detection since sensitivity of the QMC bolometer declines rapidly when operating below 70 GHz. Even at higher frequency bands (110 and 220 GHz), employment of the MVNA for detection results in poor sensitivities. Hence, for the great majority of our multifrequency high-field experiments, we mainly employed the QMC helium cooled bolometer detector in combination with the Gunn diode-based microwave oscillators equipped with appropriate Schottky diode harmonic generators (spectrometer configuration 1).

2. *Field Linearity and Calibration*

Field linearity can be defined as a statistical deviation from the relationship $B_0/I =$ constant, where I is the magnet current and B_0 is the field generated by it. For the main set of coils (this set of coils is used when the desired sweep range is larger than ± 0.1 T) we measured the field linearity by acquiring EMR signals from a small amount of a thoroughly ground polycrystalline DPPH. The suitability of using DPPH samples as field markers for high-resolution high-field EMR spectroscopy up to 16.5 T/465 GHz was established in our previous study (*41*). In order to observe DPPH-related EMR features in the field sweeping range of 8.25 T, we used the 110-GHz Gunn diode oscillator that, in combination with the Schottky diode harmonic generator, also produced second and third harmonics of its nominal frequency. Two wide-scan EMR traces resulting from sweeping the main coil from 3.5 to 12 T (lower trace) and from 12 to 3.5 T (upper trace) are shown in Fig. 6. Due to the relatively fast sweeping rate, the DPPH spectral features occurring at the corresponding resonant fields are strongly distorted and represented by narrow spikes in both traces. Nonetheless, such sharp EMR lines provided convenient field markers for calibration of the main set of coils. The feature at ca. 3.9 T was excited by the nominal frequency, $f_G = 109.33$ GHz, of the Gunn oscillator. Peaks at ca. 7.8 and 11.7 T corresponded to the second and third harmonics of f_G, respectively. We were also able to observe two additional resonant transitions that occurred around ca. 5.85 and 9.75 T. These features were produced by the fractional harmonics, $1.5\, f_G =$ 164 GHz and $2.5\, f_G = 273.3$ GHz, that were also present in the output of our 110-GHz source. [The Gunn diode used in this experiment is a "second harmonic extraction type" oscillator

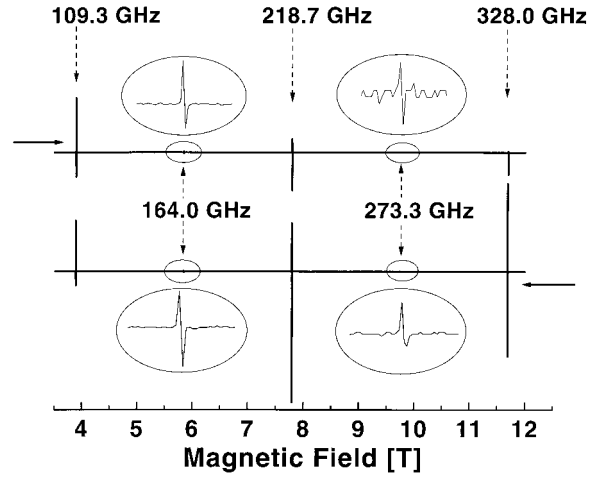

FIG. 6. Upfield and downfield EMR traces of the polycrystalline DPPH standard sample obtained using the ESA1-110 microwave source in the magnetic field range of 3.5 to 12 T (upper trace) and 12 to 3.5 T (lower trace). The main coil was used for sweeping. For both wide-scan spectra, the field sweep was stopped briefly at 6 T in order to remove or attach the harmonic generator producing the second and third harmonics of the ESA1-110 source. The major resonant transitions, depicted as narrow spikes in this wide-scan representation, were excited by the nominal frequency of the ESA1-110 source, $f_G =$ 109.3 GHz, and by its two higher harmonics, 218.7 and 328.0 GHz, respectively. The much weaker EMR features occurring around 5.85 T and 9.75 T were generated by the fractional harmonics of f_G, i.e., by 164 GHz ($1.5\, f_G$) and 273. 3 GHz ($2.5\, f_G$), respectively. These latter spectra disappear in the baseline noise of the wide-scan traces and are shown in blow-up next to the corresponding resonant fields. Experimental conditions were sweep rate, 0.1 T/min; modulation frequency, 8 kHz; modulation amplitude, 0.1 mT; time constant, 0.1 s; sample temperature, 273 K.

TABLE 3
Comparison of the Detectable Minimum Number of Spins for the Different Configurations of the HF-EMR System

Configuration	Frequency [GHz]	Sensitivity [spins/G · s]
2	24	ca. 10^{15}
2	33	ca. 10^{14}
3	110	ca. 10^{16}
4	220	ca. 10^{15}

that, in addition to its nominal frequency, f_G, also radiates weak microwave power at 1.5 f_G = 164 GHz. In combination with the nonlinear Schottky diode harmonic generator, this setup produces other fractional harmonics, including 2.5 f_G.] Although very weak, the EMR signals excited by the microwave frequencies of 164.0 and 273.3 GHz, could be retrieved from the baseline noise of both traces. After being enlarged, they are shown in Fig. 6 next to their corresponding resonant fields. The resonance field values were calculated using the resonance condition formula that involves the microwave radiation frequency and the known g-factor of DPPH standard. The corresponding magnet currents were calculated based on the manufacturer's calibration factor (0.124675 T/A). A straightforward linear fit gave the following: B_0 [T] = (0.12470 ± 0.00002) I [A], yielding field linearity of 0.02 mT/A. Additionally, by running the spectra in both directions, we also measured the field hysteresis. The effect of the field hysteresis in our magnet is mainly due to the presence of the superconducting switch and resistor-diode protection circuits. The magnitude of the field hysteresis was sweep rate dependent, ranging from ~1.5 to ~10 mT for sweeping rates of 0.01 to 0.1 T/min. When using the main coil and sweeping the magnet in both directions the committed error was found to be less than 5 mT at the sweep rate of 0.1 T/min (an averaged value was taken for the resonance field). One can reduce this error by using slower sweep rates.

A polycrystalline sample of magnesium oxide diluted in calcium oxide was used as a field marker to calibrate the field linearity of the sweeping coil. [The sweeping coil in our HF-EMR system is employed when the total sweep range does not exceed ±0.1 T, i.e., in high-resolution experiments.] The dilute MnO/CaO standard is often used for g-factor and field calibration purposes and provides the well-known sextet of narrow hyperfine features of Mn^{2+} with a linewidth of 0.1 mT (*42, 43*).

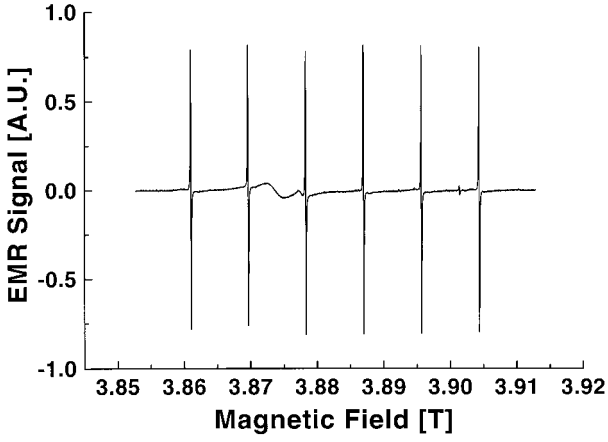

FIG. 7. EMR spectrum of Mn^{2+} center in the polycrystalline MnO/CaO standard sample recorded using the FP resonator operating at 109.71 GHz in the magnetic field sweep of 0.06 T. The main coil was kept in the persistent mode at 3.85 T. Instrumental settings were sweep rate, 0.0012 T/min; modulation frequency, 0.7 kHz; modulation amplitude, 0.025 mT; time constant, 0.3 s; sample temperature, 274 K.

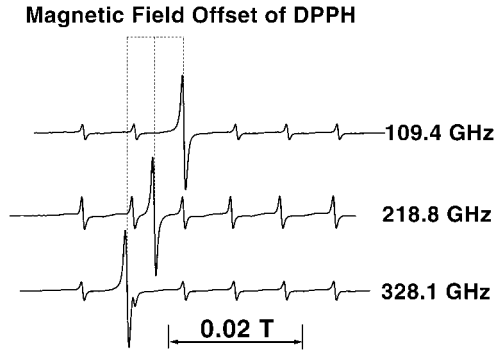

FIG. 8. Relative offset of the resonant magnetic field of DPPH in respect to the sextet of the hyperfine features of Mn^{2+} in polycrystalline MgO/MnO. The partly overlapped EMR spectra of both samples were recorded at three microwave frequencies: 109.4, 218.9, and 328.1 GHz. Instrumental settings were magnetic field sweep of 0.06 T; modulation frequency, 8 kHz; modulation amplitude, 0.025 mT; sample temperature 274 K.

The corresponding spectrum acquired in the sweeping range of 0.06 T and using the FP resonator operating at 108.71 GHz is shown in Fig. 7. The g-factor and A hyperfine constant for this standard sample were also determined from the EMR spectra measured at X band, yielding g = 2.0011 and A = 8.623 mT. We followed a similar method to that described above for field calibration of the sweeping coil. The calculated field linearity of the sweeping coil was of 0.06 mT/A. The hysteresis of the sweep coil was found to be substantially smaller than for the main coil, achieving its smallest value of ~0.3 mT when the main set of coils was set to persistent mode, independent of the actual field intensity.

3. g-Factor Resolution for Different Frequencies at High Magnetic Field

In order to check the power of the g-factor resolution of our MF HF-EMR system we acquired spectra from two standard samples. We used polycrystalline DPPH and manganese oxide diluted in magnesium oxide (0.05% of MnO in MgO) having distinct and well-known g-factor values: g_{DPPH} = 2.0036 and $g_{Mn(II)}$ = 2.0011, respectively. Both standards were positioned in the same sample compartment, thus making it possible to observe simultaneously their partly overlapped EMR spectra. At a chosen microwave frequency, f_R, the difference in the resonance fields, ΔH_R, for both standard samples is given by $\Delta H_R = (hf_R/\beta)[g_{DPPH}^{-1} - g_{Mn(II)}^{-1}]$, where h and β are Planck's constant and the Bohr magneton, respectively. At f_R = 9.5 GHz (X band), ΔH_R is small (of 0.00042 T) and the resonance field of DPPH occurs between the third and fourth hyperfine lines of Mn^{2+}. At millimeter and submillimeter frequencies, as is shown in Fig. 8, the spectral shifts are much more marked. As a result of this, the DPPH feature overlaps with the third hyperfine line of Mn^{2+} in the trace recorded at 109.4 GHz. For

the EMR traces acquired at 218.8 and 328.1 GHz, the spectral shift is even more pronounced, ΔH_R being 0.0096 T and 0.0144 T, respectively. This illustrative result points to an objective of using the multifrequency high-field approach for studying spin systems with complex or overlapped EMR spectra.

IV. APPLICATIONS

The multifrequency high-field EMR apparatus that is operational at the NHMFL in Tallahassee, Florida, has already been applied for solving a large number of different problems. In the following we present exemplary illustrations of its performance in applications that benefited from the power of the multifrequency and high-field approach. More details concerning the various experiments can be found in the cited references. All spectra presented in this section are single-trace (nonaveraged) EMR measurements and the corresponding instrumental settings are given in the figure legends.

1. Antiferromagnetic Resonance in Canted Antiferromagnets

One of the major advantages of the multifrequency high-field EMR spectroscopy is a possibility of studying the spin systems that are EMR-silent at conventional frequencies and fields. Antiferromagnetic resonance, a branch of EMR technique, is a powerful tool that provides a microscopic insight into the magnetic structure of the spin-ordered state. It enables one to investigate the magnetic exchange and anisotropy interactions, as well as to characterize spin-flop mechanisms and spin canting in aniferromagnetically coupled spin systems. However, AFMR studies have long been restricted by technical difficulties associated with working at high magnetic fields. Furthermore, the necessity of operating in a broad band of high frequencies, the prerequisite factor for successful observation of AMFR-related transitions, has also discouraged interest in this technique. We applied our EMR spectrometer to observe antiferromagnetic resonance transitions in a class of magnetically ordered manganese phosphonates. Exemplary spectra acquired for manganese phenylphosphonate [$Mn(O_3PC_6H_5) \cdot H_20$] are shown in Fig. 9. At 5 K, i.e., well below the Néel temperature for this compound, $T_N = 12.1$ K, the AFMR transitions occur in a wide spectrum of millimeter and submillimeter frequencies and in a magnetic field range of 0.3 to ca. 14 T. We employed both 95 and 110 GHz operating Gunn diode microwave sources in combination with appropriate harmonic generators for producing the following microwave frequencies: 189.9, 225.4, 284.8, 325.3, and 379.8 GHz. The QMC bolometer was used for signal detection (spectrometer configuration 1). The spectrum occurring around 1 T and at 66.7 GHz was measured using the MVNA as the microwave source and the QMC bolometer as the signal detector (spectrometer configuration 2). As shown in the inset of Fig. 9, the observed transitions fall into distinct branches of AFMR

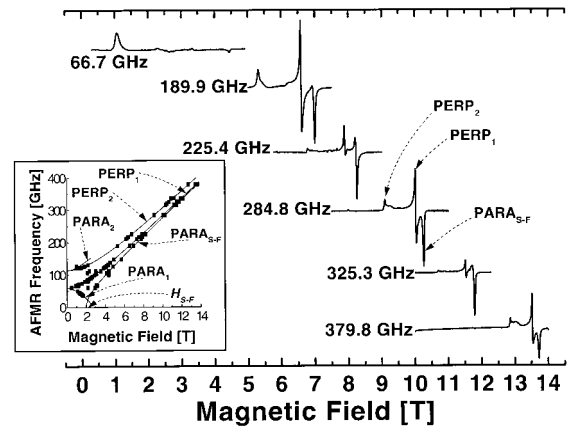

FIG. 9. Multifrequency AFMR spectra detected for manganese phenylphosphonate, ($Mn(O_3PC_6H_5) \cdot H_2O$), recorded below the antiferromagnetic ordering temperature, T_N. The three dominant peaks in the high-frequency range (189.9 GHz and higher) represent three distinct AFMR modes: two perpendicular ($PERP_1$ and $PERP_2$), and one spin-flop ($PARA_{S\text{-}F}$), respectively. The EMR spectra were acquired using spectrometer configuration 1. The trace at 66.7 GHz was recorded in the sweep range of 0.5 to 5 T, while using spectrometer configuration 2. Inset: frequency and field dependence of the AMFR transitions and their theoretical fits. Instrumental conditions were modulation frequency, 4 kHz; modulation amplitude, 1.0 mT; sample temperature, 5 K.

modes. The experimental points and theoretical fits shown in this inset represent a characteristic pattern for the frequency-field dependence of an orthorhombic antiferromagnet with two parallel ($PARA_{1,2}$) and two perpendicular ($PERP_{1,2}$) branches. At magnetic fields above a critical field determined as the spin-flop field, $H_{S\text{-}F}$, the third branch of high-field transitions occurred. These latter transitions were assigned as a parallel spin-flop branch ($PARA_{S\text{-}F}$) and could also be followed up to ca. 13.8 T. Due to the capability of observing AFMR resonances in an exceptionally wide range of electromagnetic radiation frequencies, as well as in broad magnetic field sweeps, we could accurately determine parameters characterizing the magnetically ordered phase in this system. The analysis yielded the exchange field, $H_E = 12.2$ T and the anisotropy fields, $H_{A1} = 0.18 \pm 0.3$ T and $H_{A2} = 0.66 \pm 0.3$ T, as well as the spin-flop field $H_{S\text{-}F} = 2.2 \pm 0.1$ T. Other anisotropy-related parameters, such as the Dzyaloshinsky-Moriya exchange term, $H_{D\text{-}M} = 0.4 \pm 0.1$ T, and the canting angle, $\beta = 0.6 \pm 0.2$ deg, were also determined. These results were made possible due to the multifrequency capability of our HF-EMR facility. A comprehensive analysis of the AFMR spectra obtained for this and similar systems of other manganese phosphonates can be found in Ref. (*33*).

2. Multifrequency High-Field EMR Approach for Increased Spectral Resolution of the g-Factor: Application for the Primary Donor $P700^+$ in Plant Photosystem I

A possibility of increasing spectral resolution of the g-factor that scales with increasing frequency has always been one of

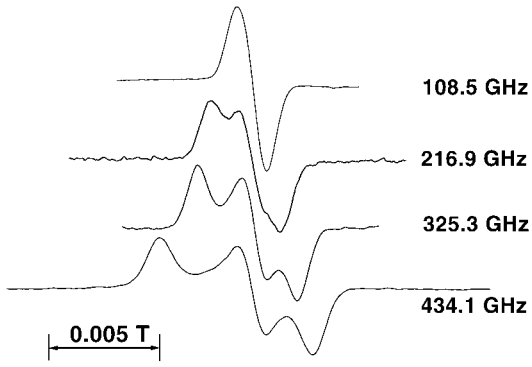

FIG. 10. EMR spectra of the light-induced chlorophyll cation radical $P700^{\bullet+}$ in photosystem I acquired at various microwave frequencies of 108.5, 216.9, 325.3, and 434.1 GHz. All EMR spectra were acquired using spectrometer configuration 1. Typical instrumental parameters were modulation frequency, 8.6 kHz; modulation amplitude, 0.5 mT; sample temperature, 5 K.

the most appealing aspects of the HF-EMR spectroscopy. Significant clarification of complex systems that have several EMR features overlapping at lower frequencies is expected from experiments performed at high fields. HF-EMR also makes it easier to analyze complex g-factor tensors, since their principal values can often be read from the high-field EMR powder spectra. Chlorophyll radicals that are involved in green plant photosynthesis are known for having complex g-factor tensors that are difficult to resolve using conventional low-field EMR technique. These radicals are considered to be primary donors in the photosystem reaction center and have been intensively studied by many research groups using a variety of spectroscopic techniques (*44–46*). They are believed to be formed by a pair of chlorophyll monomers and reveal a strong g-factor anisotropy due to delocalization of the unpaired electron between the two halves of the radical complex. We applied our MF HF-EMR system to characterize the electronic structure of such a radical system while investigating the cation radical $P700^{\bullet+}$, i.e., the primary electron donor in plant photosystem I. Light-induced EMR spectra of $P700^{\bullet+}$ acquired at 5 K in the frequency range of 108.5 to 434.1 GHz are shown in Fig. 10. We employed the 110-GHz Gunn diode oscillator in combination with the appropriate harmonic generator for recording the high-field spectra. The QMC bolometer was used for signal detection (spectrometer configuration 1). The EMR spectrum recorded at the lowest frequency (108.5 GHz) is essentially a featureless Gaussian envelope resulting from unresolved g-factor anisotropy and unresolved hyperfine interactions. In contrast, the EMR trace recorded at the higher harmonic (216.9 GHz) reveals the presence of underlying partly resolved spectral components. The traces acquired at 325.3 and 434.1 GHz reveal three distinctive components, thus showing the first well-resolved chlorophyll radical spectra observed without prior deuteration. The resolved EMR features obtained at higher frequencies enabled one to fully resolve the anisotropy of the principal elements of the g-matrix. Detailed analysis of the anisotropic g-values, as well as their correlation with the electronic structure of the dimer chlorophyll of the primary donor in plant photosystem I, was described in Ref. (*47*). These high g-factor resolution EMR experiments, possible only at high magnetic fields and at microwave frequencies higher than 300 GHz, are the starting point for a more complete study of chlorophyll g-tensors as a function of electron delocalization in various chlorophyllic systems.

3. *Application of the Multifrequency Strategy to Systems with Large Zero Field Splitting*

Paramagnetic systems with an integer electronic spin and large zero field splitting (ZFS) are often EMR-silent at conventional frequencies. Many metalloproteins contain metal ions with such an even number of electrons ($S = 1, 2, \ldots$) or contain ion clusters which interact to give a total even electron system and thus integer spin (*48, 49*). Such systems, referred to as non-Kramers centers, often reveal ZFS energies larger than the microwave quantum ($h\nu$) in conventional EMR spectrometers [$h\nu$ is $\sim$0.3 cm^{-1} at X band and $\sim$1.2 cm^{-1} at Q band, respectively.] Thus, large ZFS systems are preferentially studied by the high-field EMR techniques although, in certain specific cases, some nominally forbidden transitions may be observed by parallel polarization (B_0 parallel to H_1) in X- and Q-band EMR experiments (*50, 51*).

Many important biological systems, such as superoxide dismutase, catalase, and photosystem II, contain mono- and polynuclear manganese Mn(III). On the other hand, simpler molecules containing high-spin manganese (d^4, $S = 2$) ion, such as Mn(III) porphyrins and phthalocyanines, have been used as building blocks of molecular magnets (*52, 53*). We applied our MF HF-EMR spectrometer to investigate a high-spin manganese Mn(III) incorporated into the molecular complex of MnIII(2,3,7,8,12,13,17,18-octakis(dimethyloamino) porphyrazine chloride. High-spin manganese ion in this complex is archetypal of the many non-Kramers spin systems. A set of exemplary EMR spectra obtained for this compound is shown in Fig. 11. The spectra were taken at low temperature ($\sim$5 K) and at high fields, where $g\beta H/kT$ and $\Delta/kT > 1$. Thus, the EMR features in Fig. 11 correspond to resonant transitions, $M_s = -2 \leftrightarrow M_s = -1$, involving the ground spin state of the $S = 2$ manifold. The 95- and 110-GHz operating Gunn diode oscillators combined with the appropriate harmonic generators were used to cover the frequency band from 220.6 to 475.0 GHz. The QMC bolometer was used for signal detection (spectrometer configuration 1). The resonant transitions were observed in the field range of 0.3 to 9.6 T. A plot of the resonant field values versus microwave frequency for the observed EMR features is shown in the inset in Fig. 11. Since no resonant transitions could be observed below 200 GHz, the multifrequency high-field approach was necessary to study this system to determine the ZFS parameters (D and E) of the $S = 2$ system spin Hamiltonian. The zero field intercept at 209.79

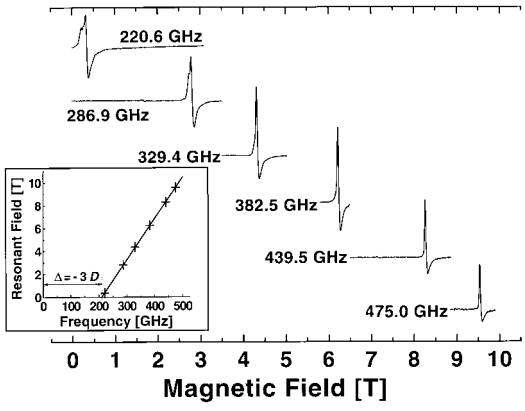

FIG. 11. Multifrequency EMR spectra of MnIII(2,3,7,8,12,13,17,18-octakis(dimethyloamino)porphyrazine) chloride measured in the frequency range of 220.6 to 475 GHz. This high-spin, $S = 2$, large ZFS spin system of Mn(III) is EMR-silent below 220 GHz. The Gunn diode sources, ESA1-95-5 and ESA1-110, in combination with appropriate harmonic generators and the QMC bolometer detector (spectrometer configuration 1), were used for acquiring the EMR spectra. Inset: experimental points (crosses) and a linear fit (solid line) of the resonant field values as a function of the resonant frequency for the observed EMR transitions. The zero field intercept of the linear fit in the inset yields the ZFS parameters $\Delta = -3D$, $D = -2.33$ cm^{-1}. Instrumental conditions were modulation frequency, 5 kHz; modulation amplitude, 1.5 mT; sample temperature, 5 K.

GHz shown in the inset in Fig. 11 determines the zero field splitting parameter $\Delta = -3D$, $D = -2.33$ cm^{-1}. On the other hand, linear dependence of the resonant field versus frequency points to an assignment of the EMR features to "parallel" transitions ($B_0 \parallel$ to z molecular axis), as well as for $E \sim 0$. Detailed analysis presenting magnetic properties of this spin system can be found in Ref. (*13*).

V. CONCLUSIONS

We built and successfully tested the multifrequency high-field EMR facility that operates in an exceptionally wide frequency range of 24 GHz to 3 THz. The heart of our MF HF-EMR system consists of the highly homogeneous Teslatron superconducting magnet that can be fast swept over the range of 0 to 15 T at 4.2 K and up to its maximum field of 17 T when cooled down to 2.2 K. In combination with a set of solid-state microwave sources, this system enables one to acquire cw HF-EMR spectra of crystalline, polycrystalline, or liquid nonlossy samples that are nonlimited in supply. Reasonable microwave power levels at the sample space and satisfactory sensitivity ($\leq 10^{11}$ spins/G · s for doped semiconductor sample at 4.2 K, and $\leq 10^{13}$ spin/G · s for polycrystalline radical samples at 273 K) were obtained for measurements performed in the frequency range of 110 to 475 GHz. For taking large magnetic scan cw EMR spectra, the main coil is employed with the maximum sweeping rate of 0.5 T/min. High-resolution narrow scans (± 0.1 T) can be acquired with the sweep coil having sweeping linearity of 500 μT/50 mT.

We explored the oversized cylindrical waveguide technology to achieve broadband performance in the whole frequency range. This approach greatly simplified the overall design of the microwave power pathway, since the technical obstacles, such as single-mode waveguide-related transmission losses and complexity of resonant sample probes, have been avoided. Simplicity of the overall spectrometer design and its satisfactory performance over an extended range of microwave frequencies and magnetic fields clearly counterbalanced its intrinsic drawbacks, such as relatively high insertion loss of cylindrical overmoded waveguides, lack of mode and phase control over the microwave pathway in transmission, and relatively low power levels at the sample space.

On selected illustrative examples, we demonstrated the potential of the multifrequency high-field EMR technique. Application of this technique has proven to be very effective in following the antiferromagnetic resonance transitions in spin-ordered layered manganese phosphonates. Therefore, the high-frequency AFMR has become a powerful technique in magnetochemical research on par with more established methods such as susceptibility and magnetization studies or calorimetry. Substantial g-factor resolution enhancement at high magnetic fields and microwave frequencies above 300 GHz resulted in the first well-resolved spectra of P700$^{\bullet}$+ cation radical in photosystem I (prior to deuteration). Employment of our MF HF-EMR apparatus for studying spin systems with large zero field splitting (non-Kramers paramagnetic species), such as porphyrins and porphyrazines containing the high-spin ($S = 2$) Mn(III) ion, also made it possible to observe resonant transitions in these otherwise EMR-silent spin systems, thus enabling one to accurately analyze their magnetic properties. In either case, a combination of the high-field EMR technology with an ultrawide band multifrequency option of our spectrometer provided a powerful tool for investigating the magnetic properties of these spin systems.

ACKNOWLEDGMENTS

The authors particularly acknowledge Mr. V. Williams from the mechanical workshop at the NHMFL for his frequent technical assistance. A.S. acknowledges the State of Florida supported NHMFL Visitors Program, Project No. 1431, and Polish KBN Grant 2-PO3B-018-13. This work was also partly supported by the Human Frontier Science Program (L.A.P.).

Note added in proof. The MVNA used in our instrument was bought in 1995. Since then, ABmm made numerous modifications that improve by two orders of magnitude the characteristics of the MVNA, when used as an EMR spectrometer.

REFERENCES

1. C. P. Poole, "Electron Spin Resonance. A Comprehensive Treatise on Experimental Techniques," Dover, New York (1983).
2. G. R. Eaton, S. S. Eaton, and K. M. Salikhov, "Foundations of Modern EPR," World Scientific, Singapore (1998).

3. O. Ya. Grinberg, A. A. Dubinskii, and Ya. S. Lebedev, *Russ. Chem. Rev.* **52,** 850 (1983).
4. E. Haindl, K. Möbius, and H. Oloff, *Z. Naturforsch.* **40a,** 169 (1985).
5. R. T. Weber, J. A. J. M. Disselhorst, L. J. Prevo, J. Schmidt, and W. Th. Wenckebach, *J. Magn. Reson.* **81,** 129 (1989).
6. W. B. Lynch, K. A. Earle, and J. H. Freed, *Rev. Sci. Instrum.* **59,** 1345 (1988).
7. F. Müller, M. A. Hopkins, N. Coron, M. Grynberg, L.-C. Brunel, and G. Martinez, *Rev. Sci. Instrum.* **60,** 3681 (1989).
8. S. S. Eaton and G. R. Eaton, in "High Magnetic Fields and High Frequencies in ESR Spectroscopy, Handbook of ESR," Vol. 2 (1996).
9. Ya. S. Lebedev, in "Modern Pulsed and Continuous-Wave Electron Spin Resonance" (L. Kevan and M. K. Bowman, Eds.), Chap. 8, Wiley, New York (1990).
10. G. Feher, *Bell Syst. Tech. J.* **36,** 449 (1957).
11. E. Rentschler, D. Gatteschi, A. Cornia, A. C. Fabretti, A. L. Barra, O. I. Shchegolikhina, and A. A. Zdanov, *Inorg. Chem.* **35,** 4427 (1996).
12. A. L. Barra, A. Caneschi, D. Gatteschi, and R. Sessoli, *J. Am. Chem. Soc.* **117,** 8855 (1995).
13. D. P. Goldberg, J. Telser, J. Krzystek, A. G. Montalban, L.-C. Brunel, A. G. M. Barrett, and B. M. Hoffman, *J. Am. Chem. Soc.* **119,** 8722 (1997).
14. K. A. Earle, D. E. Budil, and J. H. Freed, in "Advances in Magnetic and Optical Resonance" (W. Warren, Ed.), Vol. 19, Academic Press, New York (1996).
15. T. F. Prisner, in "Advances in Magnetic and Optical Resonance" (W. Warren, Ed.), Vol. 19, Academic Press, New York (1996).
16. J. Allgeier, J. A. J. M. Disselhorst, R. T. Weber, W. Th. Wenckebach, and J. Schmidt, in "Modern Pulsed and Continuous-Wave Electron Spin Resonance" (L. Kevan and M. K. Bowman, Eds.), Chap. 6, Wiley, New York (1990).
17. A. K. Hassan, A. L. Maniero, H. van Tol, C. Saylor, and L.-C. Brunel, *Appl. Magn. Reson.* **16,** 299 (1999).
18. H. Ohta, M. Sumikawa, M. Motokawa, H. Kikuchi, and H. Nagasawa, *J. Phys. Soc. Jpn.* **65,** 848 (1996).
19. A. L. Barra, D. Gatteschi, and R. Sessoli, *Phys. Rev. B* **56,** 8192 (1997).
20. M. A. Ondar, A. A. Dubinskii, O. Ya. Grinberg, J. A. Grigoriev, L. B. Vlodarskii, and Ya. S. Lebedev, *Zhurnal Strukturnoi Khimii* **22,** 59 (1981).
21. J. B. Mock, *Rev. Sci. Instrum.* **31,** 551 (1960).
22. P. R. Elliston, G. J. Troup, and D. R. Hutton, *J. Sci. Instrum.* **40,** 586 (1963).
23. J. A. J. M. Disselhorst, H. van der Meer, O. G. Poluektov, and J. Schmidt, *J. Magn. Reson. A* **115,** 118 (1995).
24. K. A. Earle, D. S. Tipikin, and J. H. Freed, *Rev. Sci. Instrum.* **67,** 2502 (1996).
25. M. R. Fuchs, T. F. Prisner, and K. Möbius, *Rev. Sci. Instrum.* **70,** 3681 (1999).
26. P. Höfer, G. G. Maresch, D. Schmalbein, and K. Holczer, *Bruker Rep.* **142,** 15 (1996).
27. D. Schmalbein, G. G. Maresch, A. Kamlowski, and P. Höfer, *Appl. Magn. Reson.* **16,** 185 (1999).
28. P. F. Goldsmith, in "Quasioptical Systems: Gaussian Beam Quasioptical Propagation and Applications" Chap. 1, IEEE Press, New York (1998).
29. M. Rohrer, J. Krzystek, V. Williams, and L.-C. Brunel, *Meas. Sci. Technol.* **10,** 275 (1999).
30. L.-C. Brunel, *Appl. Magn. Reson.* **11,** 417 (1996).
31. A. K. Hassan, L. A. Pardi, G. B. Martins, G. Cao, and L.-C. Brunel, *Phys. Rev. Lett.* **80,** 1984 (1998).
32. J. Telser, L. A. Pardi, J. Krzystek, and L.-C. Brunel, *Inorg. Chem.* **37,** 5769 (1998).
33. G. F. Fanucci, J. Krzystek, M. W. Meisel, L.-C. Brunel, and D. R. Talham, *J. Am. Chem. Soc.* **120,** 5469 (1998).
34. A. Jánossy, F. Simon, T. Fehér, A. Rockenbauer, L. Korecz, C. Chen, A. J. S. Chowdhury, and J. W. Hodby, *Phys. Rev. B* **59,** 1176 (1999).
35. G. M. Smith, J. C. G. Lesurf, R. H. Mitchell, and P. C. Riedi, *Rev. Sci. Instrum.* **69,** 3294 (1998).
36. J. T. Cardin, S. V. Kolaczkowski, J. R. Anderson, and D. E. Budil, *Appl. Magn. Reson.* **16,** 273 (1999).
37. K. A. Earle and J. H. Freed, *Appl. Magn. Reson.* **16,** 247 (1999).
38. G. Annino, M. Cassetari, I. Longo, M. Martinelli, P. J. M. Van Bentum, and E. Van der Horst, *Rev. Sci. Instrum.* **70,** 1787 (1999).
39. M. Seck and P. Wyder, *Rev. Sci. Instrum.* **69,** 1817 (1998).
40. P. Goy, unpublished experimental results.
41. J. Krzystek, A. Sienkiewicz, L. A. Pardi, and L.-C. Brunel, *J. Magn. Reson.* **125,** 207 (1997).
42. O. Burghaus, M. Rohrer, T. Gotzinger, M. Plato, and K. Möbius, *Meas. Sci. Technol.* **3,** 765 (1991).
43. B. R. McGarvey, *Trans. Met. Chem.* **3,** 89 (1966).
44. J. R. Norris, R. A. Uphaus, H. L. Crespi, and J. J. Katz, *Proc. Natl. Acad. Sci. USA* **68,** 625 (1971).
45. M. Plato, K. Möbius, and W. Lubitz, in "Chlorophylls" (H. Sheer, Ed.), p. 1015, CRC Press, Boca Raton, FL (1991).
46. H. Käss, E. Bittersman-Weidlich, L.-E. Andreasson, B. Bönigk, and W. Lubitz, *Chem. Phys.* **194,** 419 (1995).
47. P. J. Bratt, M. Rohrer, J. Krzystek, M. C. W. Evans, L.-C. Brunel, and A. Angerhofer, *J. Phys. Chem. B* **101,** 9689 (1997).
48. M. P. Hendrich and P. Debrunner, *Biophys. J.* **56,** 489 (1989).
49. T. Yamauchi, H. Mino, T. Matsukawa, A. Kawamori, and T. Ono, *Biochemistry* **36,** 7520 (1997).
50. D. T. Petasis and M. P. Hendrich, *J. Magn. Reson.* **136,** 200 (1999).
51. K. A. Campbell, E. Yikilmaz, C. V. Grant, W. Gregor, A.-F. Miller, and R. D. Britt, *J. Am. Chem. Soc.* **121,** 4714 (1999).
52. J. S. Miller, J. C. Calabrese, R. S. McLean, and A. J. Epstein, *Adv. Mater.* **4,** 498 (1992).
53. J. S. Miller, C. Vasquez, J. C. Calabrese, R. S. McLean, and A. J. Epstein, *Adv. Mater.* **6,** 217 (1994).